Analysis of Shell and Roller Failure in Dryer Section of a Paper Mill

Pal S.S.*, Grewal G.***a), Sidhu R.K.**, Sood** D., Singh S.** and Saproo R.K.*

ABSTRACT

This paper presents the results of study undertaken to investigate a catastrophic failure which recently occurred in the machine house of a modern integrated pulp and paper mill. This failure, which was specifically located in the dryer section of a paper machine, involved the simultaneous, sudden, fracture of a felt roller and two associated dryer shells. Based on a comprehensive analysis combining a number of techniques including visual, optical, scanning electron microscopy as well as computations of the stress state, the seemingly independent failure events of the two dryer shells and the felt roller were found to be closely interrelated. It was further deduced that the felt roller first underwent fatigue failure in the rotating bending mode followed by seizure and complete large scale rupture of the dryer shells.

INTRODUCTION

Recently, in the dryer section of machine #3 at the Ballarpur pulp and paper mill, a catastrophic failure occurred. The failure was accompanied by a loud tearing sound, characteristic of metal components rubbing at high velocity and pressure; and possibly undergoing rapid, unstable, fracture in a grossly brittle mode. Immediately, the machine which was running at an angular velocity of 440 RPM, was hand-tripped and the dryer section was investigated. The investigations revealed that dryer shell numbered 16 and 18 were completely ruptured. In addition, bottom dryer screen, doctor holders of the two dryer shells, and the felt roll stretcher assembly were found to be badly damaged. Further, felt roller number #33, located between the two ruptured dryer shells was found broken in two pieces. A schematic diagram showing the relative orientation of the two dryer shells and the felt roller is given in Fig. 1. The relative location of the P.V. (Pocket Ventilation) duct is also shown in this diagram. The front end of the felt roller, measuring about 700 mm. in length was found lying on the operating floor while the other portion of the roller had fallen on the ground floor. To determine the cause of this failure, a comprehensive failure investigation was undertaken. Details are presented in the following sections.

* **Ballarpur Paper Mills, Ballarpur Industries Limited, Maharashtra - 442 901, India.**

** **Thapar Corporate Research & Development Center, Bhadson Road, P. Box No. 68 Patiala - 147 001, India**

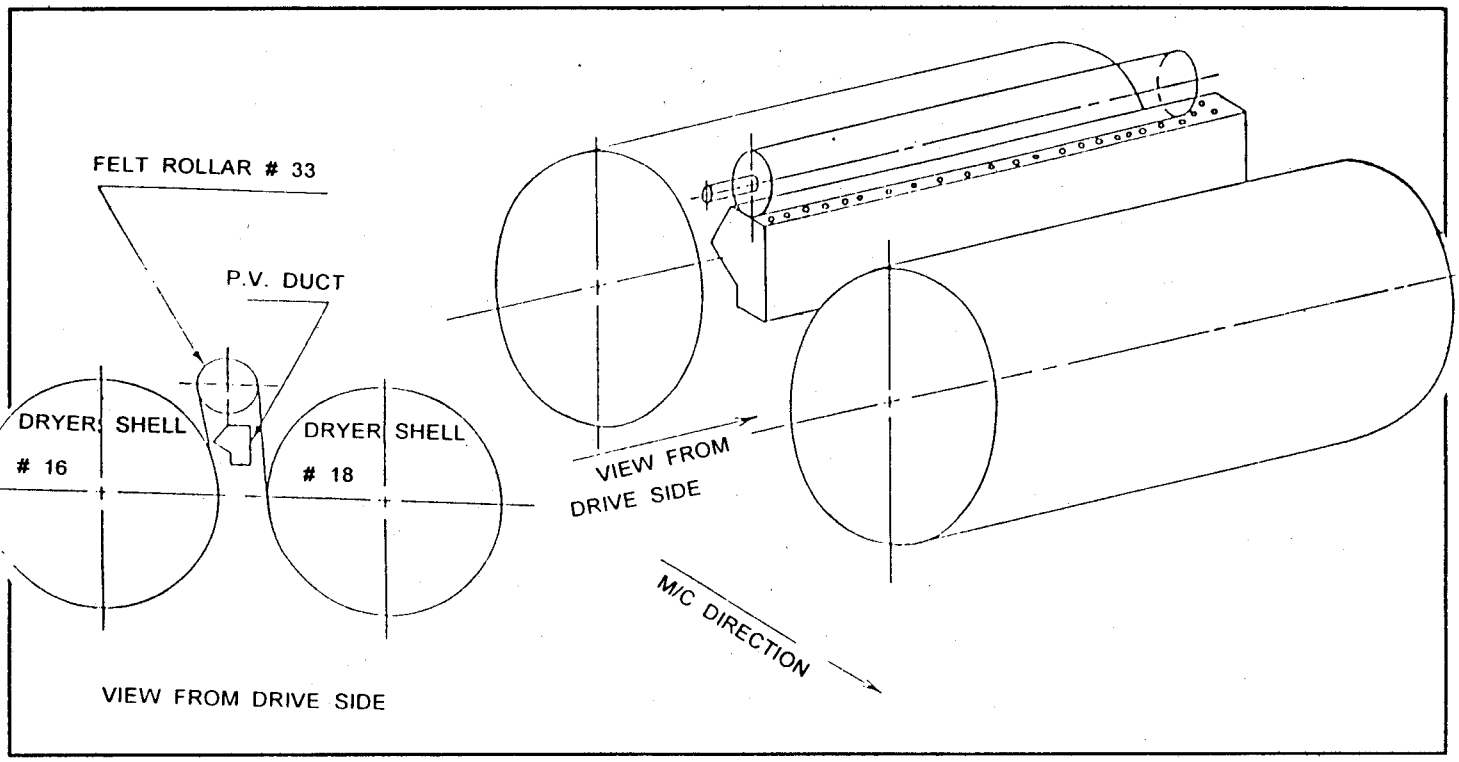

Fig. 1: A schematic diagram showing the relative configuration of the three dryer section components prior to failure

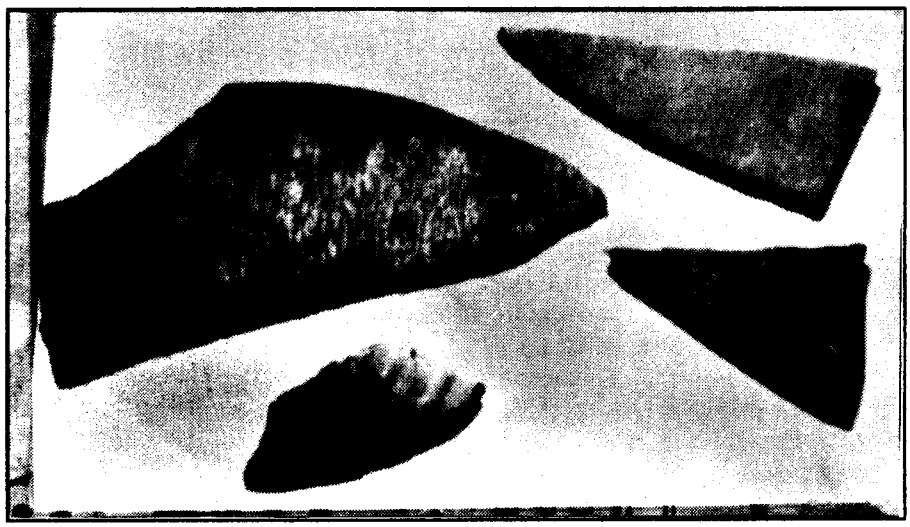

Fig. 2: Photograph showing fractured pieces of the dryer shell

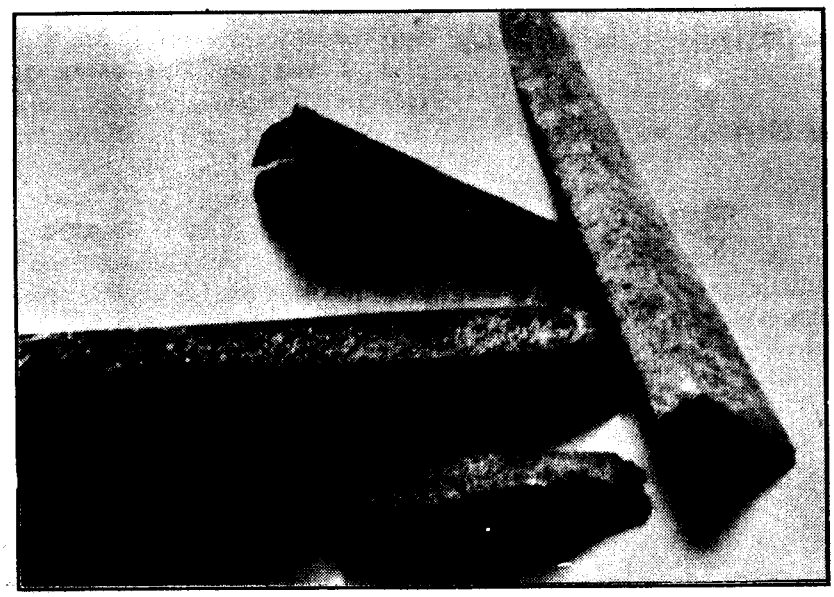

Fig. 3: Photograph showing another perspective of the fractured pieces of the dryer shell.

EXPERIMENTAL, ANALYSIS OF EVIDENCE AND DISCUSSION

Visual analysis

Representative failed pieces of the two dryer shells and the felt roller were visually examined with the aid of a low power hand held magnifying glass. The central observations of this examination are detailed below:

Dryer shell

Typical fractured pieces of the two dryer shells are shown in Figs. 2 and 3. Note the characteristic angular failure profile of all the fractured spieces shown. Examination of the concave (steam) side of the shell revealed corrosion deposit in the form of iron oxide scale. The scale was found to be quite thick in some regions.

Felt roller

The two fractured faces of the failed felt roller are shown in Fig. 4. The presence of multiple, beach marked, fatigue segments on the fracture surfaces are clearly evident in this micrograph. Further, note that the repeat period of the beach markings is quite coarse (of the order of a millimeter). this relatively large repeat period is also clearly evident in the close-ups shown in Figs. 5 and 6. Nearly seventy percent of the fracture surface was found to be beach marked indicating that structural integrity of the felt roller had been completely lost resulting in a complete fracture into two pieces, by a switching over of the crack propagation mode from that of fatigue to that of static overload. A slightly higher magnification examination with a hand-held magnifying glass also revealed the presence of cracks lying parallel to the beach marks. These cracks were found to run all the way to the outer surface, where they found intersected by longitudinal cracks, running parallel to the axis of the felt roller. However, it must be pointed out that the cracking was observed in only a few localized regions on the fatigued surface.

An examination of the points of origin of the fatigue segments indicated the cracks to have initially propagated on non axial planes (planes with normal. axis lying at an angle with respect to axis of symmetry of the felt roller). Further, the crack initiation points were found located very close to a weldment deposit, which had been placed on the inner surface of the felt roller for the purpose of dynamical balancing.

The visual evidence thus clearly suggests that the felt roller failed by a time dependent, fatigue based, damage nucleation and propagation mechanism.This suggestion was subsequently confirmed by a higher magnification micro-examination carried out using optical metallography as well as by scanning electron microscopy. Details

of this examination are presented in the following section.

Optical and scanning electron microscopy

Dryer shell

The steam sides of the two dryer shells were initially examined optically in the un-etched condition. For this purpose, the scale deposit on the steam side was first removed by mechanical scraping. Subsequently, sections of the exposed surfaces were ground and polished using standard specimen preparation techniques. Optical examination indicated the presence of carbon in the form of ASTM type-A graphite flakes, see Fig. 7. This observation confirmed the dryer shell material to be gray cast iron. Further, optical examination indicated the steam side surfaces to be extensively crated with graphitization pits. A typical observed graphitization pit is imaged in Fig. 8. Such graphitization pitting is usually found on cast iron surfaces exposed to

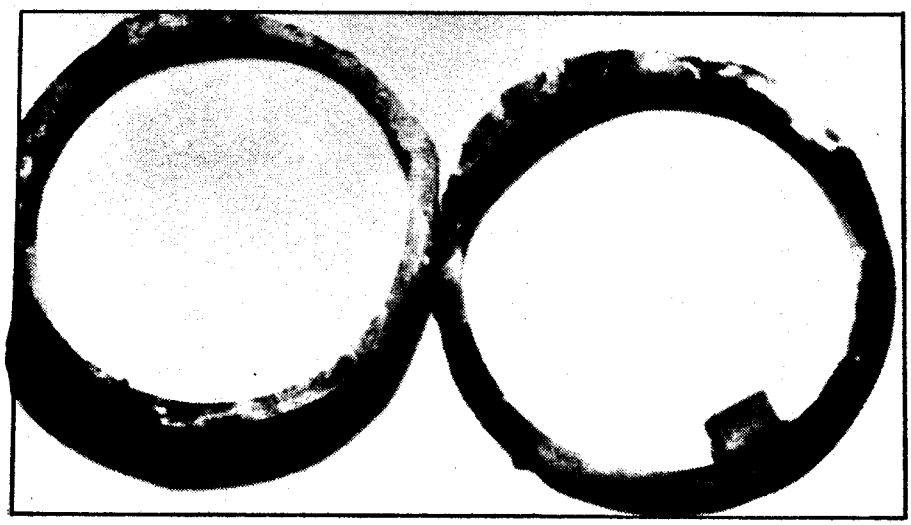

Fig. 4: Photograph showing fractured faces of the felt roller.

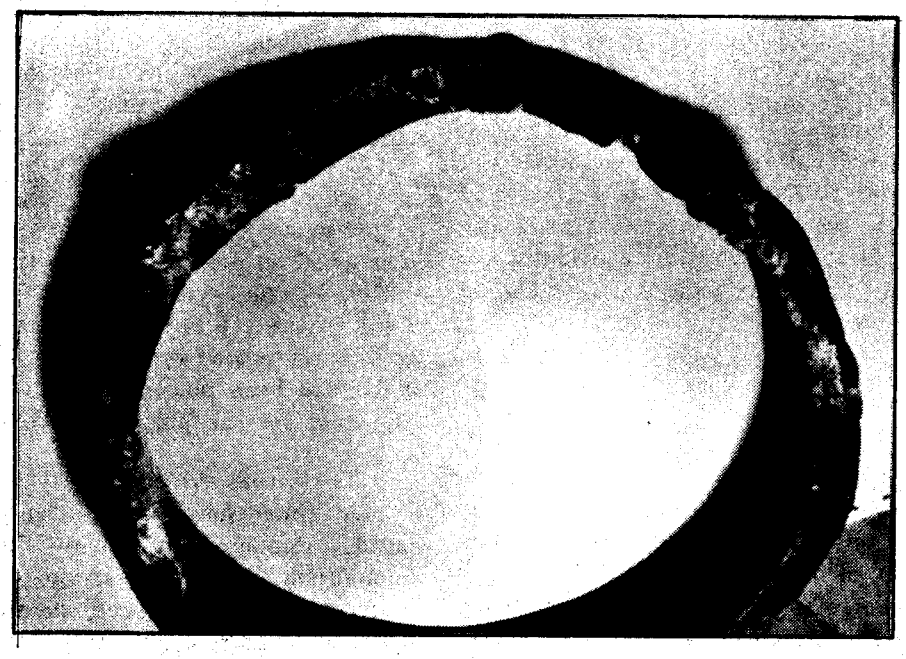

Fig. 5: Photograph showing a close-up view of the fractured face of the felt roller.

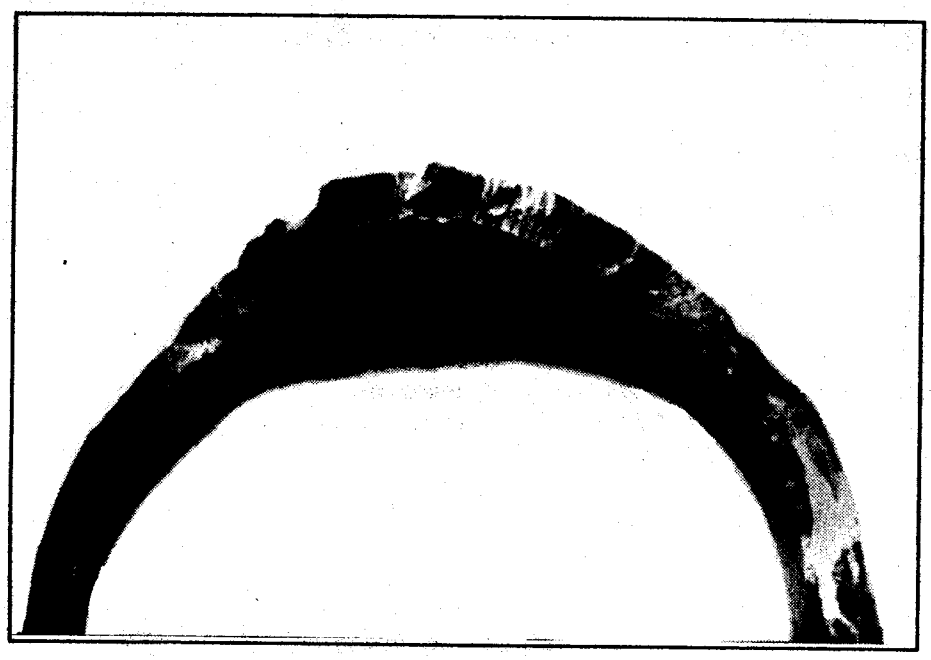

Fig. 6: Photograph showing a close-up view of the fatigue zone on the felt roller.

Fig. 7: An un-etched micrograph showing the flake morphology of dryer shell material, magnification = 100 X.

Fig. 8. An un-etched optical micrograph showing the presence of a graphitization pit on the steam side of dryer shell, magnification = 100 X

mildly oxidizing conditions over prolonged periods of time (1). To determine if the presence of graphitization pitting would compromise the structural integrity of the shell, an order of magnitude, first cut stress analysis was carried out. This analysis indicated that for the steam pressure existing in the shells, the wall thickness reduction due to the largest observed pit would have an insignificant affect on the average stress state existing in the dryer shell walls.

On completion of the examination in the un-etched condition, the microstructure of the matrix phase was revealed using a standard etching solution, see Figs. 9-10. The micrograph given in Fig 9 clearly reveals the microstructure to be predominantly pearlite with an additional presence of elongated islands of

Fig. 9: A low magnification optical micrograph showing graphite flakes and etched matrix constituents including pearlite and a ternary eutectic of steadite, magnification = 100 X..

Fig. 10 A high magnification optical micrograph showing a large island of steadite in a pearlitic matrix, magnification = 400 X

a ternary iron phosphide based eutectic called steadite. A higher magnification micrograph of an island of steadite is given in Fig. 10. The intentional presence of this eutectic phase is known to provide optimal resistance to wear and contact fatigue (2).

Scanning electron microscopy was carried out to characterize the topography of the fracture surface and graphitization pitting. Topographic details of a typical surface region pitted by graphitization are shown in the SE micrograph given in Fig 11 (12 X)

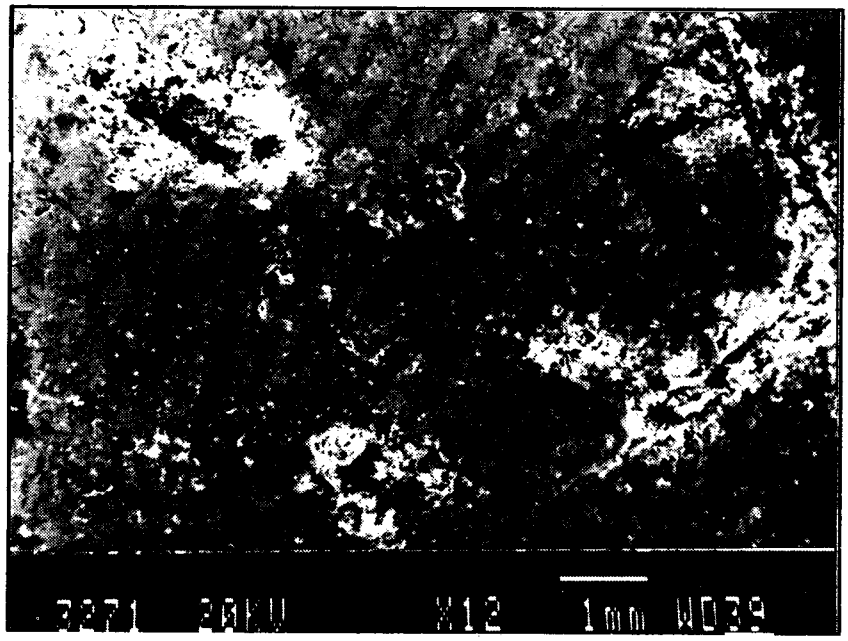

Fig. 11: A SEM micrograph showing the topography of graphitization pits.

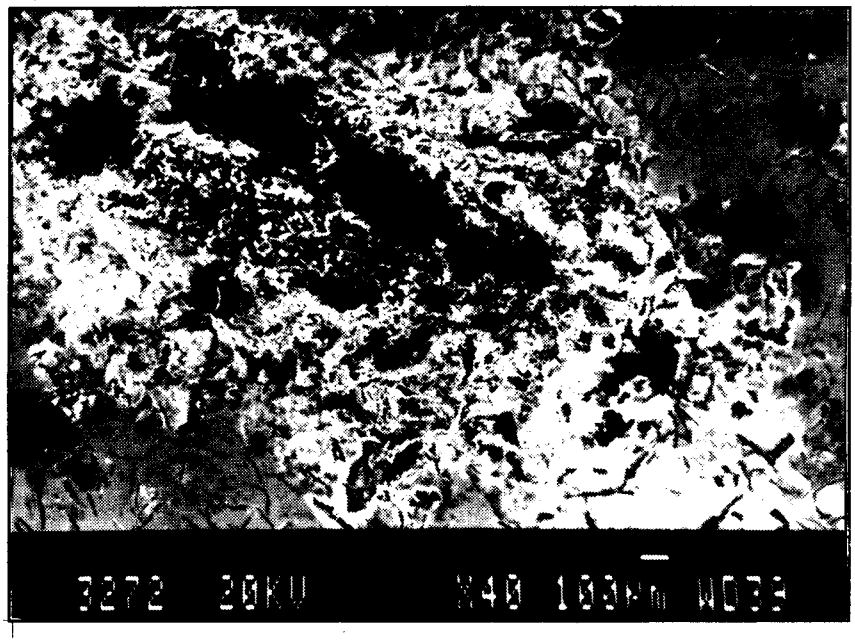

Fig. 12: A higher magnification (40 X) SE micrograph showing topography of a typical graphitization pit.

and in a slightly higher magnification SE micrograph (40 X) shown in Fig. 12. Further, a SE micrograph showing the typical topography of the fracture surface is given in Fig. 13. A higher magnification SE

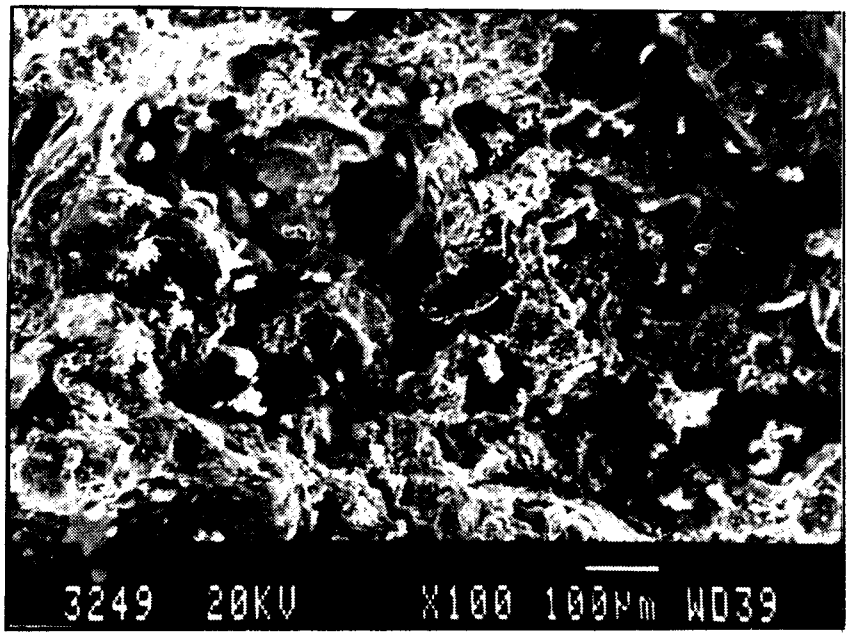

Fig. 13: A SE micrograph showing the topography of the fractured surface of the dryer shell.

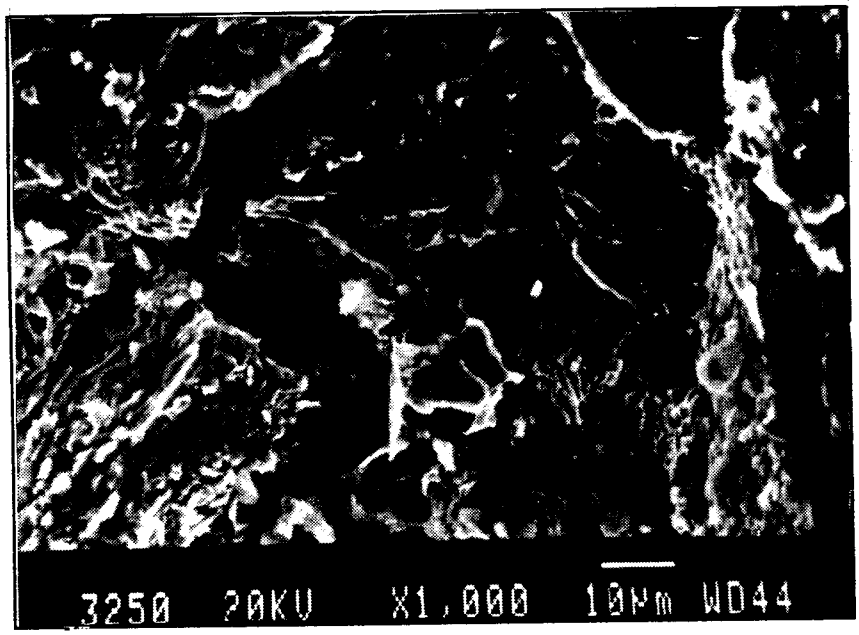

Fig. 14: A high magnification SE micrograph showing river marked fracture facets on the fracture surface of the dryer shell.

micrograph showing cleavage planes, crack separating ledges, and river markings, is given in Fig. 14. The low strain, brittle, nature of the failure is markedly evident in this micrograph. Clearly, these observations show that failure of the two dryer shells occurred as a consequence of nucleation and propagation of brittle cracks, possibly, throughout the wall volume of the two dryer shells.

Felt roller

An optical micrograph showing the microstructure of the felt roller is given in Fig. 15. The predominantly bright constituent in this

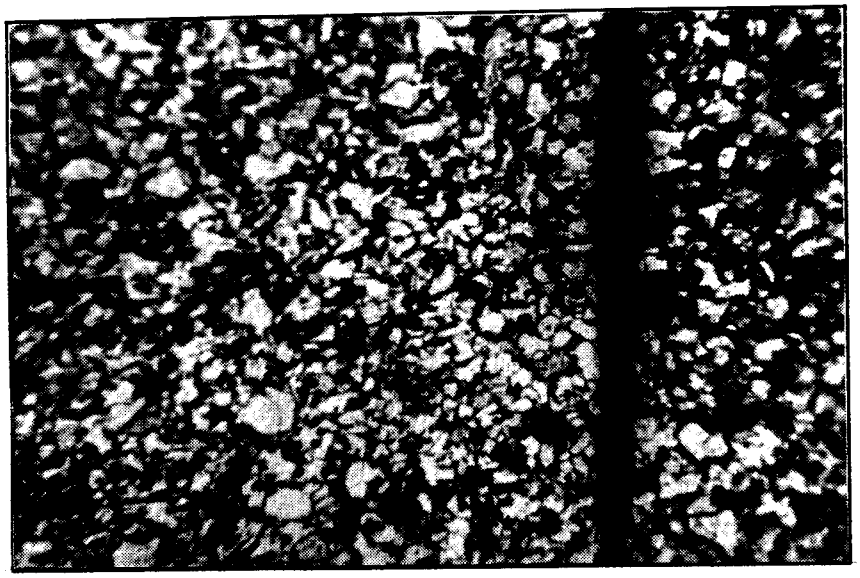

Fig. 15: An optical micrograph showing the microstructure of the felt roller material, magnification = 200 X.

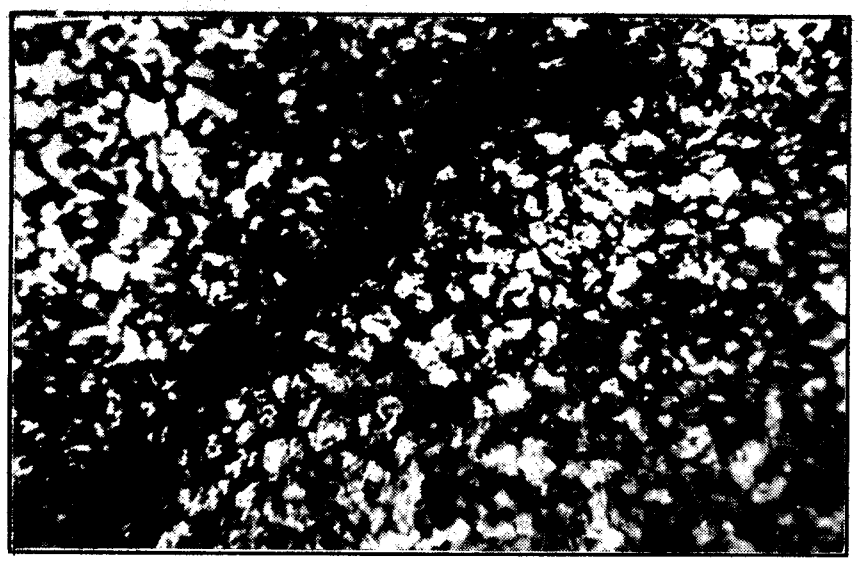

Fig. 16: An optical micrograph showing the morphology of a typical longitudinal crack found near the fatigue zone of the felt roller, magnification = 200 X.

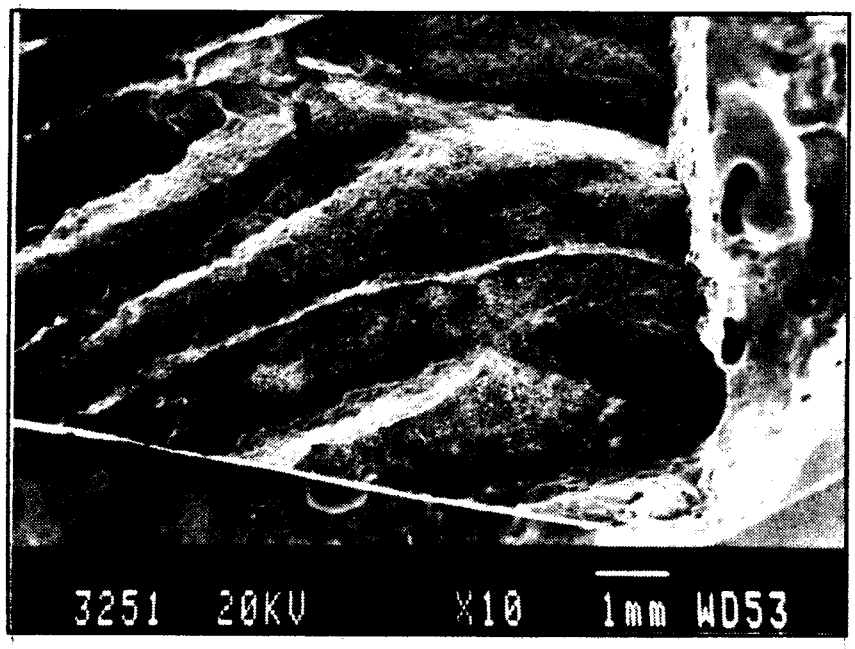

Fif. 17: A SE micrograph showing the topography of the fatigue zone in the felt

micrograph is ferrite while the darkly etching regions correspond to pearlite, In the micrograph given in Fig. 16, a typical longitudinal crack (mentioned in the previous section on visual examination) is imaged. Note that the crack appears to have propagated fairly deeply into the section shown.

Finally, in Figs. 17 and 18, SE micrographs of the fatigue surface are shown. Specifically, Fig. 17 shows the origin of the fatigue crack while Fig. 18 shows the terminal region of a fatigue segment. Optical and scanning electron microscopy thus clearly confirms the failure mechanism to be that of rotating bending fatigue.

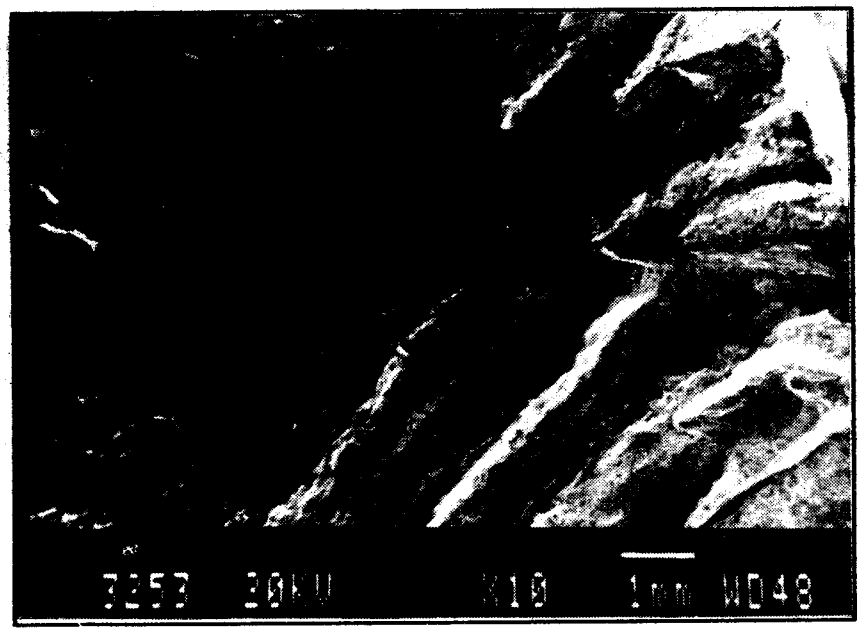

Fig. 18: A SE micrograph showing the topography of the terminal section of a fatigue segment on the fracture surface of the felt roller.

Chemical analysis and mechanical property evaluation

Chemical analysis

Drillings were obtained from the failed sections and subjected to wet chemical analysis. The results are presented in Tables 1-2, for the felt roller and the dryer shells (chemistry of the both the shells was identical), respectively. Based on these results, the felt roller material was classified as a high manganese structural steel while the dryer shell was classified as gray cast iron. The chemistry of both these materials was found to be in exact conformance with the material specifications listed in the original design data sheets for the two respective components.

Table 1: Wet chemical analysis of felt roller.

Element	Mass %
C	0.10
Si	0.34
Mn	1.32
P	0.012

Table 2: Wet chemical analysis of dryer shell

Element	Mass %
C	2.90
Si	1.05
Mn	0.67
P	0.20

Hardness and tensile property evaluation

Standard grinding and polishing techniques were used to prepare the component surfaces for sub-size Brinell hardness measurement. Based on a number of indentations, the hardness of the felt roller and the dryer shells was determined, respectively, as BHN 168 ± 9 and 186 ± 7. These values are typical hardness numbers usually reported for the two respectively materials.

The tensile strength of the dryer shell material was also determined using standard ASTM tensile specimens. These specimens were fabricated from the largest available failed pieces of the dryer shell. Based on these tests, the average tensile strength of

both the dryer shells was determined as 200 Mpa. This value was subsequently used for calculating the magnitude of the critical stress state in dryer shells.

Numerical computations of the stress state

To quantify and correlate the observed failure mechanisms with the existing stress state in the two dryer shells and the felt roller, recourse was taken to stress analysis. The various structural-cum-operational parameters, used in this analysis, are given in Tables 3 and 4, for the dryer shells and felt roller, respectively. Using this data and by assuming appropriate loading and geometrical models for the two components, the following computations were made:

Table 3: Operational and geometrical parameters of the dryer shell.

Heated length, mm	3900
Wall thickness, mm	21.3
Outer diameter, mm	1500
Angular velocity, RPM	160
Steam temperature, °C	150°C
Steam pressure, Kgf/cm²	1.8 (g)
Maximum Steam pressure, Kgf/cm²	3.0 (g)

Table 4: Operational and geometrical parameters of felt roller

Length, mm	4100
Wall thickness, mm	14.50
Outer diameter, mm	1268
Angular velocity, RPM	550
Felt tension, N/cm	24.5

Dryer shell

The state of stress existing in the dryer shell was quantified by the following computations:

1. Membrane stresses due to internal pressure, using two dimensional linear elastic theory for thin walled cylinders (4).

2. Centrifugal loading due to axial rotation of the dryer shell, using formulations of thin disk theory (4).

3. Plane-stress fracture toughness parameter, K_c, for the listed working pressure for various hypothetical configurations of surface flaws. As a typical example, calculations were performed using idealized penny shaped - "hacksaw" - crack configurations. Analysis was also attempted using idealized geometrical models of the observed graphitization pits (5, 6).

These calculations indicated the value of the plane-stress fracture toughness parameter (stress intensity factor), K_c to be extremely small. Similarly, the values for the centrifugal stresses (σ_{rr} and $\sigma_{\theta\theta}$) were found to be negligible (of the order of a fraction of one Mpa). In contrast, membrane stress computations predicted slightly higher values of about 10 Mpa for $\sigma_{\theta\theta}$, and about 5 Mpa for σ_{zz}. However, both these values are only a small fraction of the fracture stress, σ_{U}, of about Mpa for gray cast iron.

Felt roller

The state of stress in the felt roll pipe was determined as below:

1. Normal, bending moment induced stress, σ_{zz} on planes normal to the axis of roller, using beam theory. The felt tension was approximated as a line load (4).

2. Cetrifugal stresses, σ_{rr} and $\sigma_{\theta\theta}$, arising from the rotation of the rollar, using thin disk theory formulations (4).

Again, the centrifugal stresses was found to be negligible (of the order of a fraction of one Mpa). However, the maximal bending moment induced normal stress, σ_{zz}, was determined to be a much higher number at about 20 Mpa. Though, a value of 20 Mpa would be of no great consequence under static load conditions, it becomes significant if the state of stress is time variant (fatigue loading) and stress concentrations are present. For the rotating felt roller, the maximal normal stress of 20 Mpa cycles between compression (-20 Mpa) and tension (+20 Mpa) at an angular frequency of 56 radians/sec. This cyclic stress range of 40 Mpa, when combined with an appropriate stress concentration factor to account for the presence

of the weldment on the inner surface of the roller can easily result in a condition where threshold stress intensity factor range, $\Delta K_{thresh.}$ is exceeded; leading to initiation of stage-I fatigue cracking.

SYNTHESIS OF EVIDENCE

Dryer shell

The major visual, optical and scanning electron microscopy based observations clearly suggested the predominant failure mode to be brittle.overload. Since stress computations predicted the state of stress to be insignificant in the shell walls, it was conjectured that the shell was subjected to a torque overload (from the drive train), due to a possible blockage or interference of its free rotation by the felt roller. To further elaborate upon this conjecture, an attempt was made to determine the maximum external (pure shear) torque required to initiate catastrophic fracture. For this purpose, pure torsion theory was invoked. Assuming the fracture stress of the cast iron to be 200 Mpa the critical value for the torque was determined to be about 15 M (NM), which appears to be a seemingly very large and implausible number. It is pertinent, however, to view this number in light of the fact that the calculation assumes a homogeneous monolithic solid, and the stress concentration due to the morphology of the graphite flakes and other defects is not accounted for. Further, the actual torque to initiate catastrophic global failure in the dryer shell would be significantly lower than this value, if a more realistic, threshold flaw size based, fracture mechanics approach were to be adopted and existence of interference contact stresses factored in.

Felt roller

The visual, optical, and scanning electron microscopy based observations clearly suggested that the failure of the felt roller occurred by fatigue. In addition, it was conclusively shown that the fatigue cracking initiated at a weldment (deposited for dynamic balancing) on the inside surface of the felt roller. A potential stress based driving force for fatigue crack propagation was also demonstrated by taking recourse to stress analysis.

CONCLUSIONS

Based on the central results obtained in this investigation, the following three stage failure scenario is proposed:

In the first stage, the felt roller, which is stationed between two dryer shells accumulated fatigue damage in the course of its normal operational life. The fatigue cracking initiated at stress concentration sites, created by a weldment deposit on the inner surface of the felt roller. As a consequence of propagation of the fatigue cracks, the felt roller lost structural integrity leading to eventual failure static overload.

The second stage initiated, possibly, much before the felt roller underwent complete static overload failure. In fact, it is reasonable to conjecture that as a consequence of fatigue crack propagation, the structural integrity and stiffness was lost to such an extent that the felt roller underwent excessive out of plane displacement, possibly in the (machine) direction of dryer shell #18. The subsequent interference of the felt roller with the P.V. vent and the dryer shell #18 then led to the complete fracture of the felt roller

In the final stage, the interference of the partially or completely fractured felt roller with dryer shell #18 led to the blockage of its free rotation. At the same time, an equally tremendous amount of contact loading would have been also transmitted to dryer shell #16 via the P.V. duct. As a consequence, a large shear moment loading rate resulted on the axial planes of both the dryer shells (in addition to the Hertzian contact stresses). As a consequence, when the principal normal stresses on the principal planes attained the fracture stress values (for a pure shear loading, the maximal principal stress is equal in magnitude to the principal shear stress), or alternatively, in a fracture mechanics interpretation, when the critical stress intensity factor for unstable crack propagation was exceeded, the entire shell structure suffered global catastrophic failure.

To mitigate the probability of such a failures from occuring again in the dryer section, recommendations were made to discontinue the use of felt rollers which had been balanced by a welding operation. Further, it was also suggested that the relatively rigid P.V. duct made out of steel be replaced by a low stiffness structure, made out of a low modulus material like aluminium. These suggestion have now been implemented at the Ballarpur plant.

REFERENCES

1. Fontana M.G., "Corrosion Engineering", Mc Graw-Hill Book Company, New York, 1987, p. 89.

2. Arzamasov B. (Editor), "Materials Science", Mir Publishers, Moscow, 1989, p. 198.

3. Fontana M.G., "Corrosion Engineering", McGraw-Hill Book Company, New York, 1987, p. 89.

4. Timoshenko S. and Goodier J.N., "Theory of Elasticity", McGraw-Hill Book Company, International Edition, Kogakusha Co. Ltd., Japan, 1951, p. 29.

5. Shigley J.E., "Mechanical Engineering Design", McGraw-Hill Book Company, International Edition, Singapore, 1986, p. 217.

6. Blake A., "Practical Stress Analysis in Engineering Design", Marcel Dekker, Inc., New York, 1990, p. 135.